USPIO-Enhanced 3D-Cine Self-Gated Cardiac MRI Based on a Stack-of-Stars Golden Angle Short Echo Time Sequence: Application on Mice With Acute Myocardial Infarction

Aurélien J. Trotier, PhD, Charles R. Castets, MSc, William Lefrançois, PhD, Emeline J. Ribot, PhD, Jean-Michel Franconi, PhD, Eric Thiaudière, PhD, and Sylvain Miraux, PhD*

Purpose: To develop and assess a 3D-cine self-gated method for cardiac imaging of murine models.
Materials and Methods: A 3D stack-of-stars (SOS) short echo time (STE) sequence with a navigator echo was performed at 7T on healthy mice ($n = 4$) and mice with acute myocardial infarction (MI) ($n = 4$) injected with ultrasmall superparamagnetic iron oxide (USPIO) nanoparticles. In all, 402 spokes were acquired per stack with the incremental or the golden angle method using an angle increment of (360/402)° or 222.48°, respectively. A cylindrical *k*-space was filled and repeated with a maximum number of repetitions (NR) of 10. 3D cine cardiac images at 156 μm resolution were reconstructed retrospectively and compared for the two methods in terms of contrast-to-noise ratio (CNR). The golden angle images were also reconstructed with NR = 10, 6, and 3, to assess cardiac functional parameters (ejection fraction, EF) on both animal models.
Results: The combination of 3D SOS-STE and USPIO injection allowed us to optimize the identification of cardiac peaks on navigator signal and generate high CNR between blood and myocardium (15.3 ± 1.0). The golden angle method resulted in a more homogeneous distribution of the spokes inside a stack ($P < 0.05$), enabling reducing the acquisition time to 15 minutes. EF was significantly different between healthy and MI mice ($P < 0.05$).
Conclusion: The method proposed here showed that 3D-cine images could be obtained without electrocardiogram or respiratory gating in mice. It allows precise measurement of cardiac functional parameters even on MI mice.

J. MAGN. RESON. IMAGING 2016;00:000–000.

Magnetic resonance imaging (MRI) has become the standard reference for assessing anatomic and cardiac functions in mice.[1] This technique provides images with a good spatial and temporal resolution and excellent endogenous contrast. In addition, due to its noninvasive nature, it can be used as part of longitudinal follow-up with disease models to obtain information on disease progression or drug responses.[2,3] However, despite hardware advances in preclinical MRI scanners with the use of high gradient strengths and phased array coils, there remain a number of limitations to image animal models of myocardial infarction (MI). Among these limitations, the corruption of the electrocardiogram (ECG) signal—due to damage of cardiac muscle associated with this disease—and the use of high magnetic field gradients hindering good cardiac and respiratory gating during MR acquisition. To overcome this problem, self-gating imaging methods (also known as wireless methods)[4,5] can be substituted for ECG and respiratory gating.

It has been shown that repeating measurements without phase encoding makes it possible to extract signal variations

View this article online at wileyonlinelibrary.com. DOI: 10.1002/jmri.25150
Received Oct 14, 2015, Accepted for publication Dec 23, 2015.
*Address reprint requests to: S.M., 146 rue Léo Saignat, 33076 Bordeaux Cedex, France. E-mail: miraux@rmsb.u-bordeaux2.fr
From the Centre de Résonance Magnétique des Systèmes Biologiques, UMR 5536 Université de Bordeaux, Bordeaux, France.
Additional supporting information may be found in the online version of this article

synchronous with cardiac motion from the raw MR data. The amplitude of this MR signal (in either magnitude or phase) changes along cardiac cycle.[6,7] Movement of the myocardium and particularly blood flow generates a strong time-of-flight effect and causes a periodic change, which is visible in the MR signal. Self-gating methods thus allow retrospective reconstruction of the images based on the cardiac cycle while also correcting for artifacts due to respiratory motion. These methods have been used both in small animals[8–11] and in humans,[7,12,13] and have more recently benefited from the flexibility provided by radial imaging methods combined with pseudorandom encoding of *k*-space.[14–18]

Other difficulties associated with imaging of small-animal models of MI are related to animal basic physiological characteristics. The rapid heartbeat and fast blood flow lead to motion and flow artifacts. In addition, the very small size of the structures to be observed requires images to be acquired at a high spatial resolution. Thus, imaging the whole heart, from the base to the apex, may require a long acquisition time, which is not realistic in studies involving fragile animals.

It was recently shown that radial acquisition methods with short or ultrashort echo times (STE or UTE) could be used to avoid numerous artifacts, in particular those linked to blood flow and movement, as well as susceptibility artifacts, which are often significant at high magnetic fields.[18–20] With 2D imaging, these acquisition methods are also compatible with retrospective self-gating techniques without further modification, since the first point on each spoke acquired contains all the information related to movement.[19] 3D image acquisition with isotropic resolutions should provide a better description of the disease models, as the volumetric measurements will be more precise than with multislice 2D imaging.[21] Numerous 3D sequences have been developed to encode the signal from the center of the *k*-space towards the exterior, and thus produce STE or UTE. These sequences include: stack-of-stars STE (3D-SOS STE),[22] 3D-spokes with Kooshball sampling,[23] stack-of-spirals,[24] 3D twisted-projection-imaging (TPI),[25] and 3D cones.[26,27] At high magnetic fields, it is preferable to use sequences with the shortest possible signal-readout times, ie, 3D-spokes or 3D-SOS UTE.

The 3D-spokes method allows isotropic acquisition and provides the shortest possible echo time, as it does not require the use of a slice selection gradient. However, it is limited to the acquisition of spherical fields-of-view and results in long acquisition times if the Nyquist criterion is to be satisfied. The 3D-SOS STE sequence is a hybrid radial-Cartesian method that uses encoding in the 2D radial (star-like shape) plane within the slice, and a Cartesian encoding in the third dimension. The echo times are longer than with a 3D-spoke-type sequence, but good resolution can be obtained in the plane without increasing the volume covered.[28] The sequence can be easily modified to register an MR signal compatible with self-gating.

The objective of this study was to develop and evaluate a 3D cine self-gated method for the assessment of the cardiac function of healthy mice and mice with acute MI.

Materials and Methods

Magnet and Gradient System

Experiments were performed on a 7T Bruker Biospec (Ettlingen, Germany) equipped with a gradient system capable of 660 mT/m maximum strength and 110 μs rise time. A volume resonator (86 mm inner diameter, active length = 70 mm) operating in quadrature mode was used for excitation, and a four-element (2 × 2) phased array surface coil (outer dimensions of one coil element: 12 × 16 mm^2; total outer dimensions: 26 × 21 mm^2) was used for signal reception.

Animal Preparation

All experimental procedures were approved by the Animal Care and Use Institutional Ethics Committee of Bordeaux, France (Approval No. 5012032-A).

Healthy ($n = 4$) and ischemic ($n = 4$) mice OF1 with body weights 37–40 g were purchased from a commercial breeder (Charles River, Paris, France). Mice were anesthetized with isoflurane (1.0–1.5% in air). The animals were positioned within the magnet with the heart placed at the center of the MR coil.

Before mice positioning in the magnet, a 150 μL volume of 200 μmol Fe/kg of ultrasmall superparamagnetic iron oxide (USPIO) (Sinerem, Guerbet, Aulnay-sous-Bois, France) was injected through the tail vein.

The average heart rate for all normal mice included in the experiment was 412 ± 32 beats per minutes and 370 ± 53 beats per minutes for ischemic mice.

Self-Gated 3D Stack-of-Stars STE sequences

A 3D self-gated SOS STE sequence was implemented as schematically shown in Fig. 1.

To minimize echo time, gradients were optimized with refocusing slice gradient and slice encoding gradient durations equal to 54 μs and 315 μs, respectively. For the navigator signal, three data points were sampled corresponding to a duration of 30 μs (3 × dwell time) during the refocusing slice gradient and before the slice encoding gradient.

In all, 402 spokes were acquired per stack with two methods: 1) the incremental method with an angle increment of (360/402)°, 2) the golden-angle method with an angle increment of 222.48°.[29] Then 96 stacks were acquired to fulfill a cylindrical *k*-space. The same scheme was repeated (NR) 10 times.

Imaging Parameters

The following acquisition parameters were used: repetition time / echo time (TR/TE) = 4.0/0.527 msec, excitation pulse/duration/flip angle = hermite/0.3 msec/15° or 4° when specified, field-of-view = 20 × 20 × 15 mm^3, matrix = 128 × 128, number of stacks = 96, number of spokes per stack = 402, receiver bandwidth = 781 Hz/pixel. Ten repetitions were performed corresponding to a total acquisition time of 25 minutes 43 seconds to reconstruct 10 images per cardiac cycle (cine).

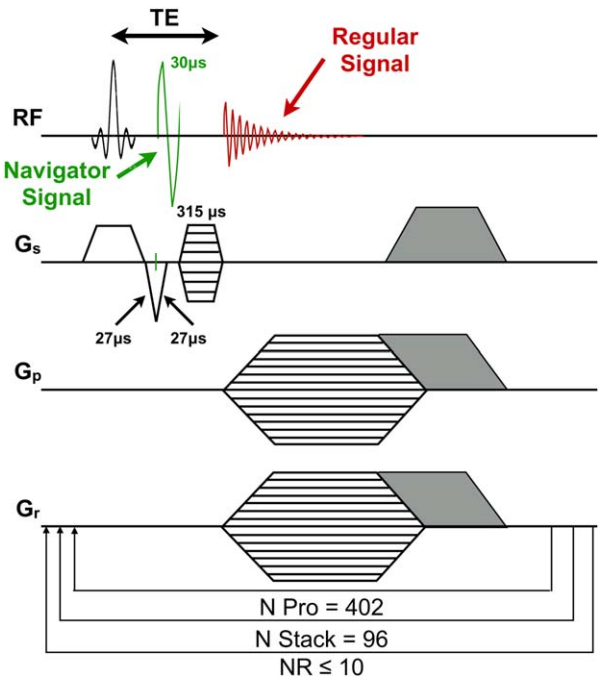

FIGURE 1: 3D SOS STE sequence and self-gated signal. The navigator echo was recorded during the slice refocusing gradient. Three points were sampled in the navigator echo signal. The duration of encoding in the slice direction was limited to 315 µs, providing an echo time of 0.527 msec. In all, 402 projections were stacked, and 96 stacks were used to generate the 3D image. The maximum NR used was 10. Spoiler gradients are indicated in gray.

Self-Gating Signal Processing

Signal processing was conducted offline with MatLab (MathWorks, Natick, MA). The three sampled navigator points were summed over each coil element. The coil element that gave the maximum amplitude was convoluted with a Gaussian filter (width = 20 points, σ value = 10). Then a peak-detection algorithm was applied to determine the start of the cardiac cycle. Median and standard deviations of the duration of the cardiac cycle throughout an experiment were calculated. Data collected in a cardiac cycle of a duration greater than or lesser than 2 times the standard deviation were discarded prior to cine reconstruction. According to their temporal position within a cardiac cycle period, the *k*-space data were attributed to the corresponding cine frame.

Comparison of Stack Encoding Mode (Incremental vs. Golden)

The two stack encoding modes (incremental and golden) were compared on data acquired on healthy mice. Shorter acquisition times were achieved by considering decreasing amounts of repetition. To compare the two methods, an analysis of the *k*-space density was performed on retrospectively reorganized data. The mean angle and its standard deviation between projections of one stack were computed for each stack and for each 3D cine image.

Reconstruction Procedure

All the STE datasets were reconstructed using the following procedure: *k*-space data were regridded with an oversampling ratio of 2 using a Kaiser-Bessel kernel.[30] Data were transformed by applying a conventional fast Fourier transform (FFT). Each phased array receiver magnitude image was reconstructed using the method described above, and then combined by a sum of squares reconstruction.

Image and Cardiac Volumetry Analysis

Signal-to-noise ratios (SNRs) were calculated according to the methods published by Kellman and McVeigh.[31] Contrast-to-noise ratio (CNR) was defined as CNR = SNR (blood) – SNR (myocardium).

Signal homogeneity of blood throughout the cycle was assessed using the measurements of the standard deviation of the blood signal from both the left and the right ventricles.

To demonstrate the improvement of image quality obtained with our method, cardiac volumetry analysis was computed per slice and per volume.

A semiautomated segmentation procedure was performed on Amira (Visage Imaging, Germany). The 3D volumes (end-diastole and end-systole) were first oriented to a short-axis view. Then the segmentation procedure was applied for each reconstructed 2D slice from the top of the heart to the apex. Left ventricle end diastolic volume (EDV), end systolic volume (ESV), and ejection fraction (EF) were computed for each slice and analysis reported either slice-by-slice or combined to obtain measurements for the whole heart.

Statistical Analysis

Results were compared using paired Student's *t*-test. $P < 0.05$ was considered significantly different.

Results

3D Self-Gated Signal

The self-gated signal obtained with the 2D version of the STE sequence without contrast agent injection and a slice thickness of 0.3 mm is shown in Fig. 2a. Cardiac and respiratory cycles could be extracted from these raw data with or without filtering and cine images could be reconstructed retrospectively. When the slice thickness is increased for 3D imaging, as shown in Fig. 2b, peaks due to respiratory motion appeared with a comparable amplitude as those obtained in 2D. On the contrary, the amplitude of cardiac peaks decreased and their level of noise was drastically enhanced. This was observed with a flip angle of 15° and 4° (Ernst angle for blood). The signal can be filtered for k-lines assignment to the corresponding cardiac time frames. However, the major problems with the 3D acquisition was the low blood signal in the left ventricle (SNR = 9.57 ± 2.19 and CNR = –7.82 ± 2.31) as shown in Fig. 2b. Cardiac volumetric analysis could not be done. After the injection of a USPIO contrast agent, blood signal in both ventricles was enhanced (SNR = 42.25 ± 2.20 and CNR = 17.25 ± 2.04), as shown in Fig. 2c. Signal intensity of cardiac peaks is increased and noise level is lower compared to data without contrast agent. Movie frames could be reconstructed after k-lines assignment and used for cardiac functional analysis. Between 5 and 10% of the total k-lines acquired during the

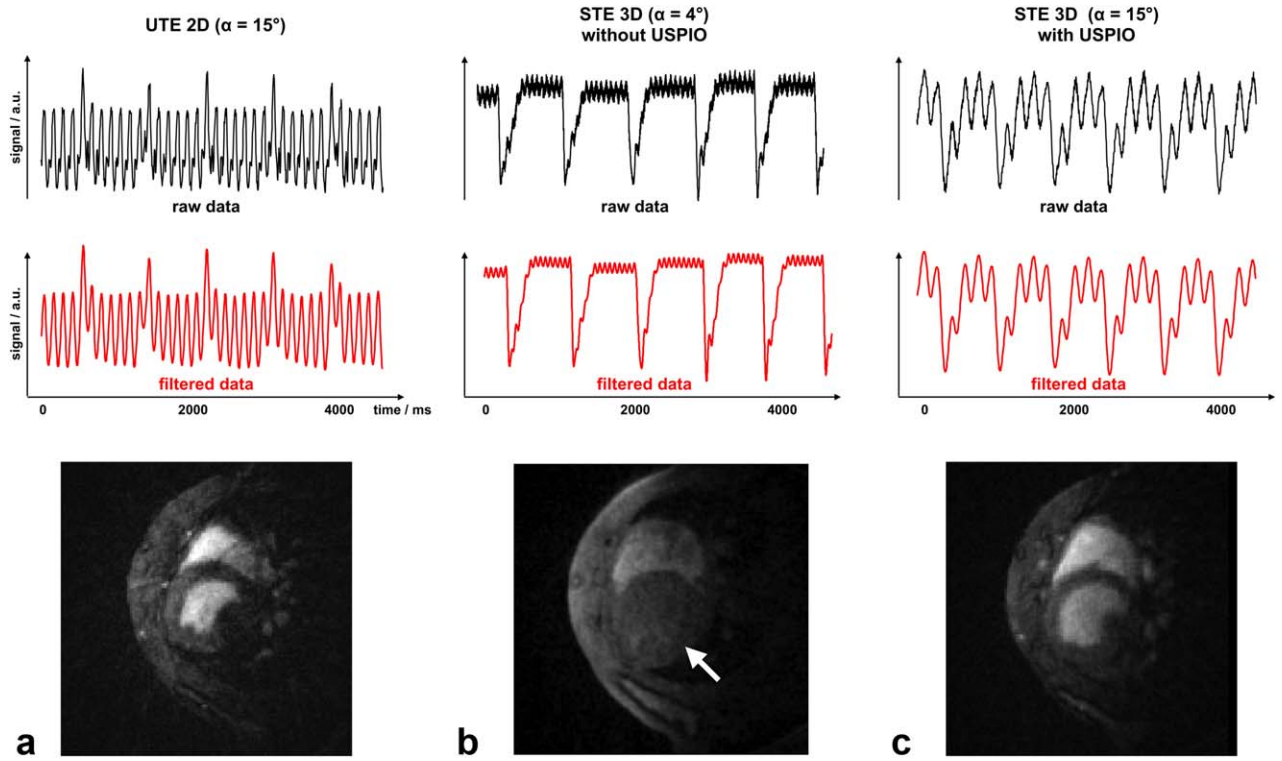

FIGURE 2: Raw and filtered navigator echo signals obtained with a 2D STE sequence (a), a 3D SOS STE sequence without injection of contrast agent (b), and a 3D SOS STE sequence with injection of iron oxide nanoparticles (c). The most intense fluctuations are typical of respiratory motion, while the least intense are characteristic of cardiac movement. The images obtained with the three sequences are shown on the bottom line. With the 3D sequence without contrast agent, a very low-intensity signal from blood was measured in the left ventricle (arrow).

experiments were rejected due to a too high standard deviation of the duration of a cardiac cycle compared to its median duration.

Stack Encoding Mode (Incremental vs. Golden Angle)

Figure 3a shows the mean value for the angle between spokes as a function of the number of repetitions (NR). The two methods provided almost identical results, with values of less than 2° for a large number of repetitions (greater than NR = 7) and values increasing to 9° for a single repetition. In contrast, the standard deviation of the angle was smaller ($P < 0.05$) when calculated using the method based on the golden angle compared to that calculated using the method based on an incremental angle (Fig. 3b). This difference in standard deviations between the methods increased as the number of repetitions decreased.

Representative magnified images reconstructed along the long and short axes are shown in Fig. 4a,b. These images were obtained on a healthy mouse with the two methods and decreasing number of repetitions used for reconstruction of cine images. With the maximum number

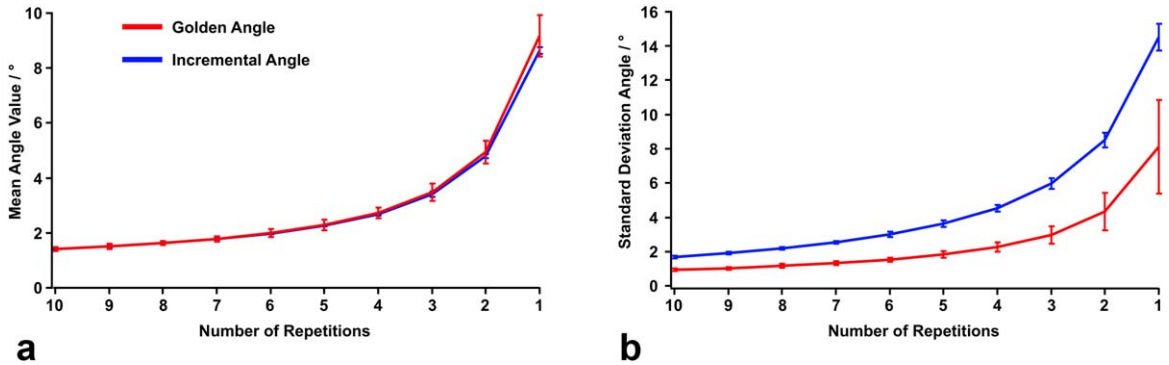

FIGURE 3: Comparison of the methods for spoke distribution within a stack: incremental angle (blue line) or golden angle (red line). a: Mean value of the angle between each of the spokes depending on the number of repetitions. b: Standard deviation for the angle between each of the spokes for different numbers of repetitions. The standard deviations are significantly different between golden angle and incremental angle ($P < 0.05$). Data shown were obtained from healthy mice.

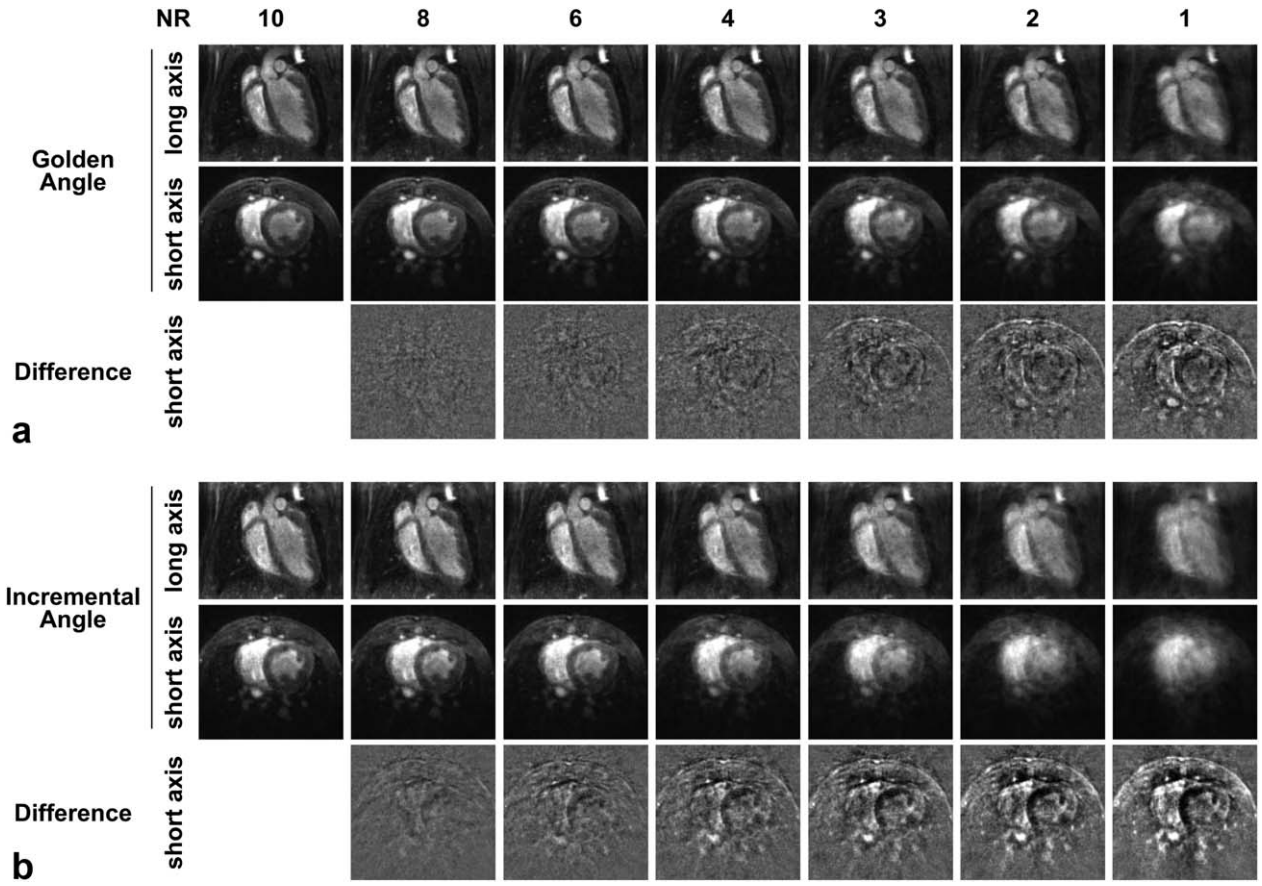

FIGURE 4: Long-axis and short-axis images of the 3D end diastolic volumes obtained with the golden-angle distribution (a) or the incremental-angle distribution (b) with varying numbers of repetitions. The difference between the images acquired with NR = 10 and the other NR values is shown for both methods along the short axis.

of repetitions (NR = 10), the images were similar in terms of SNR and CNR. The signal for blood within the heart appeared homogeneous in the left ventricle (SD = 1.56) and with very slight heterogeneity in the right ventricle (SD = 2.81) which might be due to the time-of-flight effect. No flow artifacts were observed in either ventricles. The CNR between blood and the myocardium was around 15 with both methods (Table 1). As the NR decreased, image quality decreased more significantly with the incremental-angle method. This can be seen by subtracting the images with a lower NR from the image with NR = 10 (called difference in Fig. 4). The spatial resolution of the images degraded and the CNR between the blood and the myocardium dropped more significantly on images obtained with the incremental-angle method (Table 1). When the number of repetitions was severely reduced (NR = 2 and 1), it was still possible to visualize the ventricles and the walls of the myocardium with the golden-angle method, but not with the incremental-angle method.

Healthy vs. Infarcted Cine Images

Figure 5 shows 10 cine images from a healthy mouse along the long and short axes with 6 repetitions. Figure 6 shows similar images acquired for a mouse with severe myocardial ischemia.

In both mice, the blood appears with an intense, homogeneous signal and no flow artifacts were present at all timepoints in the cardiac cycle. The 3D acquisition enabled

TABLE 1. Contrast-to-Noise Ratio (CNR) Between Blood in the Left Ventricle and Myocardium for Images Obtained With Projections Distributed Using Both Golden-Angle and Incremental-Angle Methods for Different Numbers of Repetitions (NR)

	NR = 10	NR = 8	NR = 6	NR = 4	NR = 3[a]	NR = 2[a]	NR = 1[a]
Golden angle	15.3 ± 1.0	13.0 ± 0.9	10.6 ± 1.2	8.9 ± 1.5	9.0 ± 1.0	9.8 ± 1.9	8.1 ± 1.8
Incremental angle	14.0 ± 0.9	10.6 ± 1.2	9.6 ± 1.8	7.5 ± 1.9	3.2 ± 1.7	5.5 ± 1.6	1.8 ± 1.9

[a]Significantly different between golden and incremental angle ($P < 0.05$).

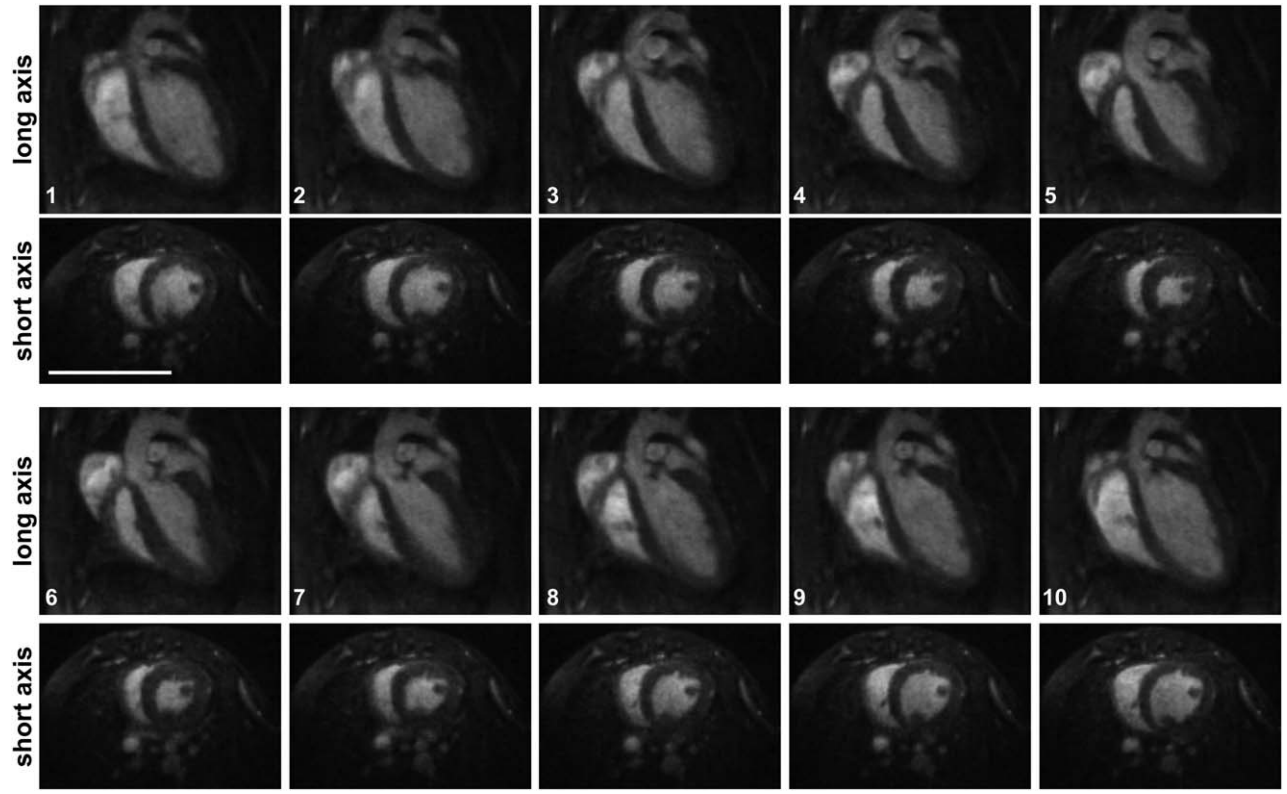

FIGURE 5: Ten 3D-cine images (along the long and short axes) obtained for a healthy mouse using the self-gated SOS STE sequence, spoke distribution based on the golden-angle method, and 6 repetitions. Scale bar = 1 cm.

a clear visualization of the whole ischemic zone as seen in the different views of the images (arrows in Fig. 6).

From these images acquired on both healthy and pathological mice, the left ventricle EDV and ESV were measured, and the EF was calculated. The mean values for the EF, EDV, and ESV for the left ventricle were significantly higher in healthy mice than in mice with MI (Table 2). These values were calculated with NR = 10.

Measurements were then made on reconstructed images with NR = 6 and 3, and compared to the reference data obtained with NR = 10. Data obtained with NR = 6 were very similar to data obtained with NR = 10 for both groups of mice. In contrast, with NR = 3 the data obtained for healthy mice appeared more widely dispersed, as shown by the Bland–Altman graph in Fig. 7. This effect was most likely due to the smaller volumes compared to those measured in ischemic mice and to the degradation of the spatial resolution on these strongly undersampled images.

Movies showing 3D-cine images from a mouse with MI are available as Supporting Material files 1–4.

Analysis of EFs for Different Heart Regions

Due to the 3D nature of the data acquired, EFs could be analyzed slice by slice from the apex to the top of the heart.

For the healthy mouse shown in Fig. 8a, the heart was thus divided into 40 slices of ~150 μm thick. The EF appeared constant throughout the long axis, with values close to the mean EF. Identical profiles were observed on other healthy mice analyzed.

For the mouse with MI shown in Fig. 8b, the heart was divided into 55 slices. Down to around slice 15 (upper heart region), the value for the EF was not statistically different from the one in healthy mice. Subsequently, it decreased strongly, becoming null from slice 40 to slice 55.

Discussion

A 3D-cine self-gated imaging method to measure left ventricle function in mice was developed and used to characterize healthy mice and mice with severe MI. Advantages of self-gating compared to prospective 2D acquisitions have already been demonstrated in murine models.[9,11,32,33] Here we developed a 3D method that was based on hybrid encoding: in-plane radial encoding with short echo times and Cartesian encoding in the slice dimension. The use of Cartesian encoding in the third dimension has several advantages: first, it enables performing relatively precise slice selection. Second, with the sequence proposed here, the navigator echo signal can be read during the gradient used for slice refocusing and thus used to generate a cardiac self-gating signal.[7] This is necessary as, unlike conventional 2D UTE sequences, the first point of the UTE signal sampled in the center of *k*-space cannot be used as a navigator echo.[18,19] It was also necessary to add encoding in the slice direction, producing a longer echo time in 3D. Nevertheless, by

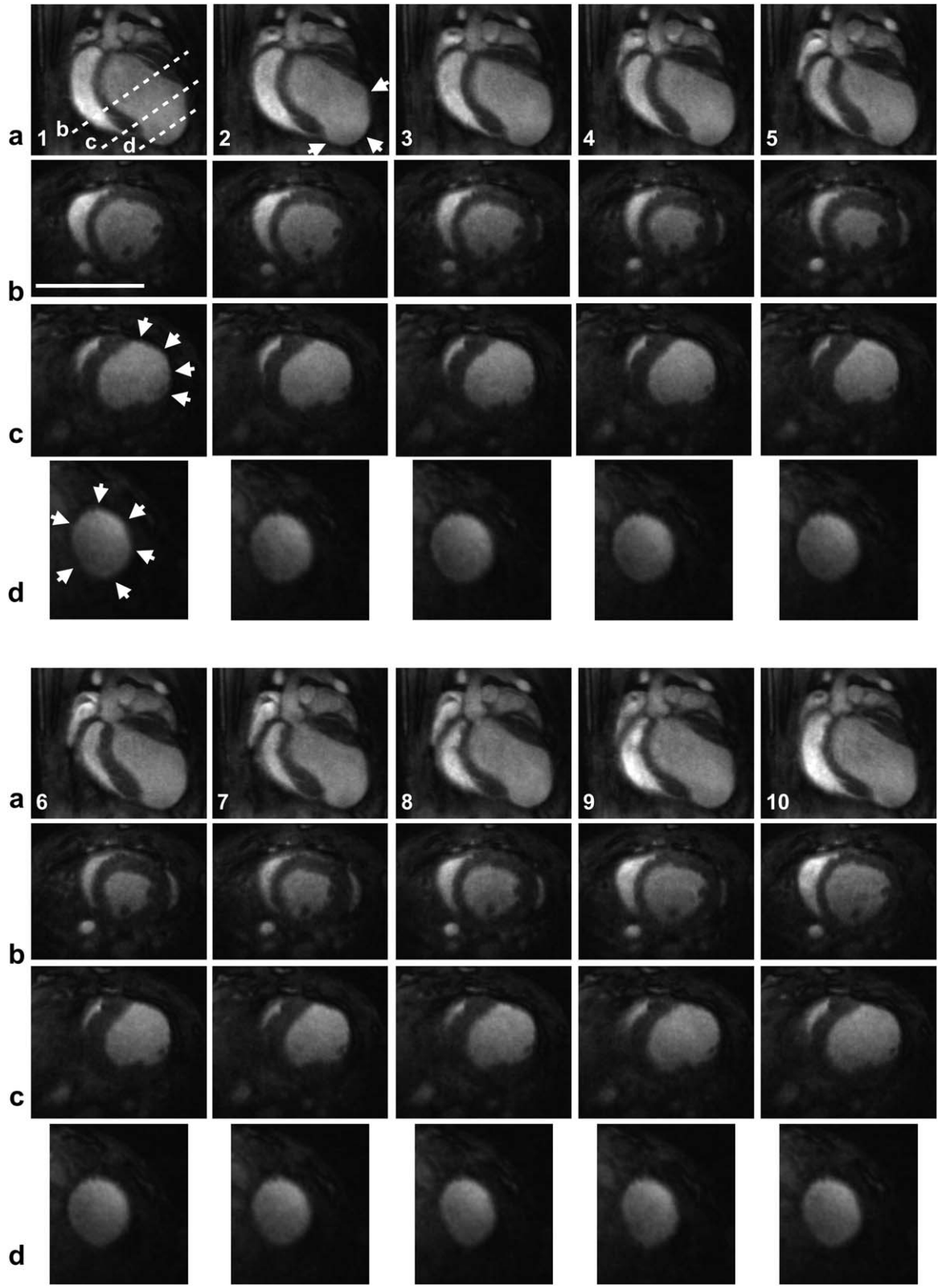

FIGURE 6: Ten 3D-cine images obtained for a mouse with MI using the self-gated SOS STE sequence, spoke distribution based on the golden-angle method, and 6 repetitions. a: Long-axis view. The positions of the slices shown in (b), (c,d) are indicated in Fig. 1a. Arrows indicate the ischemic zone. Scale bar = 1 cm.

Compressing the sequence and applying high encoding gradients, it was possible to limit the echo time to around 0.5 msec. With this method, as already proposed with 2D sequences, the navigator echo signal can be read at each TR. This contrasts with other studies performed in humans[34,35] and small animals[16] where the navigator echo signal is only read

TABLE 2. Mean Ejection Fraction (EF), End Diastolic Volume (EDV), and End Systolic Volume (ESV) for Healthy Mice and Mice With Myocardial Infarction

	EF(%)[a]	EDV (μL)[a]	ESV (μL)[a]
Healthy mice	67.7 ± 4.4	42.1 ± 7.1	13.7 ± 3.8
Mice with MI	20.7 ± 4.7	147.1 ± 19.2	116.1 ± 15.4

[a]Significantly different between healthy mice and mice with MI ($P < 0.05$)

periodically (every 4 or 10 TR). In mice, where the heart beats very rapidly, this repeated reading of the navigator echo signal allows to precisely identify the cardiac gating signal.

The other advantage of this sequence using Cartesian encoding in the slice direction is that the field of view in the third direction, and therefore the acquisition time, is reduced. However, despite a slice of relatively low thickness, the signal from blood present in the heart cavities appeared saturated in mice without a USPIO injection. Blood could not be clearly visualized in the left ventricle, unlike with 2D acquisitions where slices are typically around 10-fold thinner and where the time-of-flight effect is observed. As in several other 3D-cine studies involving small animals, it was therefore required to enhance the signal for the blood by using a contrast agent.[36,37] As described previously, an iron-based contrast agent was used.[20] These contrast agents have the advantages of showing a strong vascular persistence and generating a positive contrast when imaged using UTE and STE sequences, even at high magnetic fields.[38] Compared to a recently published study using a 3D nonselective UTE sequence,[20] the echo time was increased here around 15-fold (TE = 0.031 msec vs. TE = 0.531 msec, respectively). Interestingly, this increase did not prevent the positive contrast induced by USPIO. The blood maintained an intense signal throughout the experiment. Even if the T_2^* value due to the presence of USPIO was around 2 msec (from blood sample data), no decrease in spatial resolution or unwanted artifact was observed. This might be due to the short readout time (700 μs) obtained with our sequence. Actually, due to the center-out encoding, the echo time for the sequence remained well below a millisecond. Moreover, this type of encoding made the sequence relatively insensitive to motion and flow artifacts, even in its 3D version. Respiratory gating was therefore not necessary. The blood signal appeared homogenous throughout the cardiac cycle in both groups of mice. This enabled performing unambiguous segmentation and precisely measuring the ventricular volumes.

STE sequences are also compatible with undersampling. As a result, it is not necessary to acquire a complete *k*-space to generate an image. Thus, in the case of a retrospective method, this encoding provides high-quality images without the need to satisfy the Nyquist criterion. Nevertheless, with a conventional incremental trajectory, the distribution of the projections was not perfectly homogeneous, particularly when a low NR was used. This resulted in the appearance of typical radial encoding artifacts (streaking artifacts). To improve this situation, a pseudorandom trajectory based on the golden angle was implemented for each stack. As shown here and demonstrated by Konstandin et al,[14] using this trajectory in combination with the retrospective reconstruction method resulted in a more homogeneous distribution of the spokes inside a stack. This enabled obtaining strongly undersampled 3D images with a better spatial resolution and could be used to reduce the acquisition time, to compensate for data loss due to a poor navigator echo signal, or to reconstruct a larger number of cine images per cardiac cycle. Other recently developed pseudorandom methods for angular increment have been developed like tiny golden anlges[39] or azimuthal equidistant projections[40] and could be interesting for our approach. In this study, pseudorandom encoding was only used inside each stack. Because of the 3D nature of the sequence, it may be possible to extend this pseudorandom characteristic between the various stacks to further limit reconstruction artifacts after undersampling (ongoing work).

By combining the different advantages of the sequence developed here, we showed that 3D-cine images could be

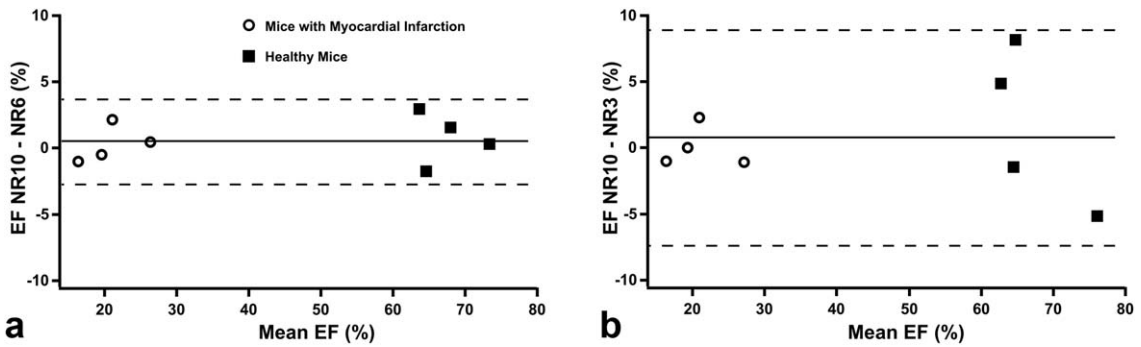

FIGURE 7: Bland–Altman graph of the EF for NR = 6 and NR = 3 compared to NR = 10. The closed squares represent data from healthy mice and the open circles show data for mice with MI.

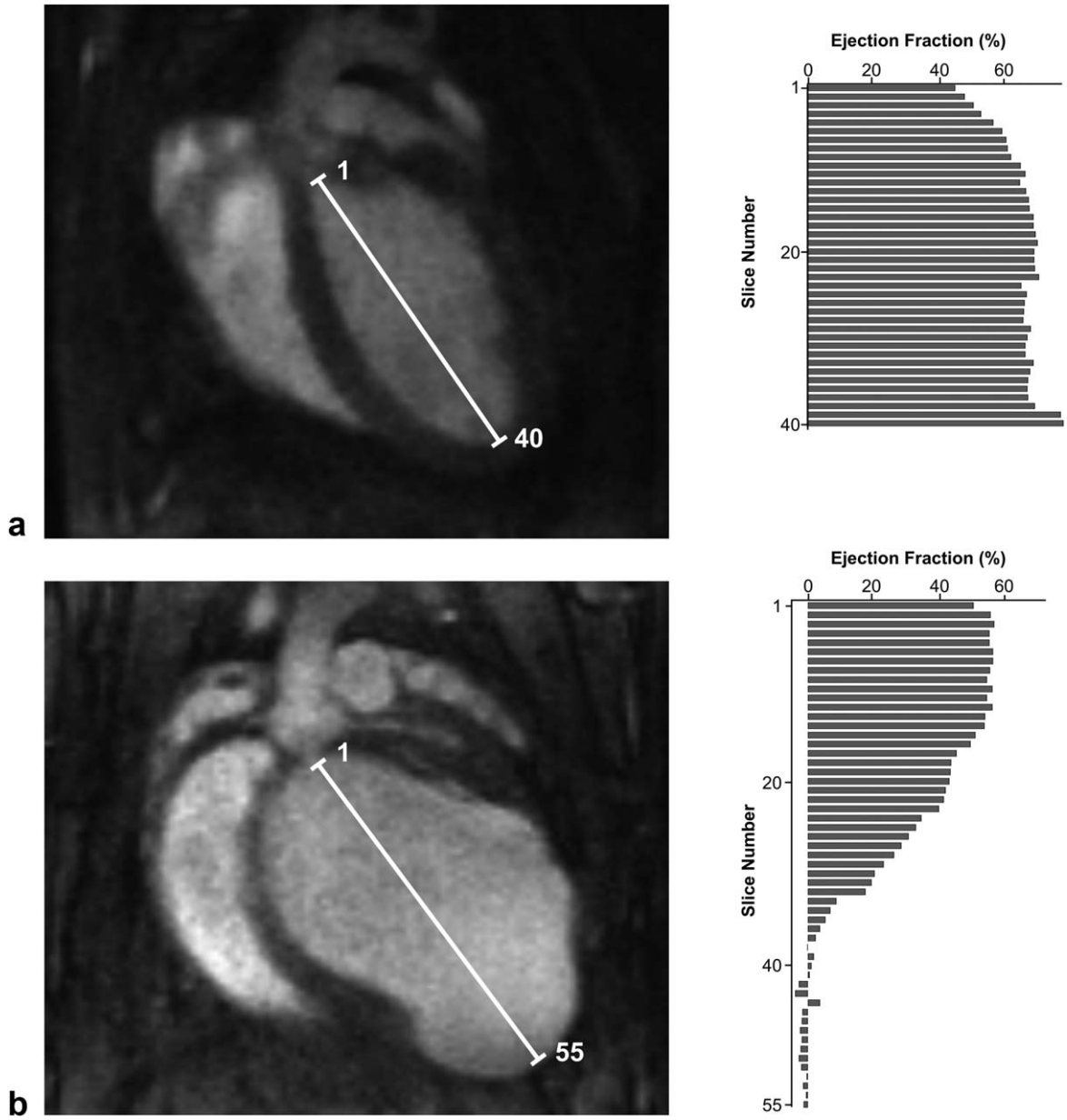

FIGURE 8: Analysis of the ejection fraction for different positions in the heart. (a) Healthy mice; (b) mice with MI. The segments on the images represent the axis along which slices were positioned. The EF was significantly different between healthy mice and mice with MI after slice number 18 ($P < 0.05$).

obtained without ECG gating, both in healthy mice and in mice with severe MI. After injecting iron oxide nanoparticles, the self-gating signal was of sufficient quality, even in mice with MI. High resolutions were obtained in the three spatial dimensions, allowing a much more precise description of the disease model than available to date in the literature.[11,18] Indeed, in these two preclinical studies, imaging was performed in 2D with a slice thickness superior to 800 μm. Bovens et al,[11] using a self-gated Cartesian FLASH sequence, obtained 17 cine-images on 11–13 slices with an in-plane resolution of 117 $\times$ 234 μm. Similarly, Motaal et al[18] performed a 2D self-gated UTE sequence on five slices to obtain 15 cine-images with an in-plane resolution of 195 μm. Here, 40 reconstructed pseudoslices were generated to determine the functional parameters of the heart in healthy mice, and even 55 slices in mice with MI. With these 3D data, functional parameters could be described globally or slice-by-slice. With the global approach, our results are in accordance with those published by Bovens et al.[11] The slice-by-slice approach used allowed us to better localize and characterize pathologies. Nevertheless, this approach has to be validated on other pathological models.

The method used here also reduced acquisition times, which is highly desirable in studies involving fragile animals. The number of repetitions was initially set to 10 (acquisition time = 25 min 43 sec), but it could be reduced to 15

minutes 26 seconds (NR = 6) without major loss of image quality. The measurements of the functional parameters remained extremely robust with this NR. When the NR was further reduced to 3 (acquisition time = 7 min 52 sec), the error increased but remained acceptable.

There are some limitations in this study. First, an injection of a contrast agent with a long blood half-life is necessary to obtain a sufficient contrast between blood and myocardium. Only iron-based contrast agents were tested. Second, due to the lack of 3D-cine cardiac imaging methods in mice, our approach was not compared to a gold-standard method. Third, fast imaging methods like a parallel imaging technique or more recent methods like compressed sensing[41] were not evaluated to further reduce total acquisition time. A standard parallel imaging technique can be performed without supplementary development due to the Cartesian encoding in the third dimension and might reduce the total acquisition time by a factor of 2. The efficiency of these techniques would be even more enhanced by the used of optimized hardware like cryo-coils.[42]

In summary, we present a method for 3D-cine imaging of mouse hearts enhanced by iron oxide nanoparticles using a hybrid radial-Cartesian sequence with short echo time. The technique combined a self-gating method with pseudorandom encoding of data to measure the functional heart parameters both in healthy mice and in mice with MI. Very high spatial resolution was achieved, and the acquisition time was limited to around 15 minutes for whole-heart coverage.

Acknowledgment

This work was supported by a public grant, Translational Research and Advanced Imaging Laboratory, which is part of the French National Research Agency's Investments for the Future Program ("NewFISP" TRAIL; ANR-10-LABX-57).

References

1. Bakermans AJ, Abdurrachim D, Moonen RP, et al. Small animal cardiovascular MR imaging and spectroscopy. Prog Nucl Magn Reson Spectrosc 2015;88–89:1–47.
2. Protti A, Lavin B, Dong X, et al. Assessment of myocardial remodeling using an elastin/tropoelastin specific agent with high field magnetic resonance imaging (MRI). J Am Heart Assoc 2015;4:e001851.
3. Holmström KM, Pan X, Liu JC, et al. Assessment of cardiac function in mice lacking the mitochondrial calcium uniporter. J Mol Cell Cardiol 2015;85:178–182.
4. Spraggins TA. Wireless retrospective gating: application to cine cardiac imaging. Magn Reson Imaging 1990;8:675–681.
5. Kim WS, Mun CW, Kim DJ, Cho ZH. Extraction of cardiac and respiratory motion cycles by use of projection data and its applications to NMR imaging. Magn Reson Med 1990;13:25–37.
6. Larson AC, White RD, Laub G, McVeigh ER, Li D, Simonetti OP. Self-gated cardiac cine MRI. Magn Reson Med 2004;51:93–102.
7. Crowe ME, Larson AC, Zhang Q, et al. Automated rectilinear self-gated cardiac cine imaging. Magn Reson Med 2004;52:782–788.
8. Hiba B, Richard N, Janier M, Croisille P. Cardiac and respiratory double self-gated cine MRI in the mouse at 7 T. Magn Reson Med 2006; 55:506–513.
9. Heijman E, De Graaf W, Niessen P, et al. Comparison between prospective and retrospective triggering for mouse cardiac MRI. NMR Biomed 2007;20:439–447.
10. Hiba B, Richard N, Thibault H, Janier M. Cardiac and respiratory self-gated cine MRI in the mouse: comparison between radial and rectilinear techniques at 7T. Magn Reson Med 2007;58:745–753.
11. Bovens SM, Te Boekhorst BCM, Den Ouden K, et al. Evaluation of infarcted murine heart function: comparison of prospectively triggered with self-gated MRI. NMR Biomed 2011;24:307–315.
12. Larson AC, Kellman P, Arai A, et al. Preliminary investigation of respiratory self-gating for free-breathing segmented cine MRI. Magn Reson Med 2005;53:159–168.
13. Ingle RR, Santos JM, Overall WR, McConnell MV, Hu BS, Nishimura DG. Self-gated fat-suppressed cardiac cine MRI. Magn Reson Med 2015;73:1764–1774.
14. Konstandin S, Nagel AM, Heiler PM, Schad LR. Two-dimensional radial acquisition technique with density adaption in sodium MRI. Magn Reson Med 2011;65:1090–1096.
15. Krämer M, Herrmann K, Biermann J, Reichenbach JR. Retrospective reconstruction of cardiac cine images from golden-ratio radial MRI using one-dimensional navigators. J Magn Reson Imaging 2014;40: 413–422.
16. Krämer M, Herrmann K, Biermann J, Freiburger S, Schwarzer M, Reichenbach JR. Self-gated cardiac Cine MRI of the rat on a clinical 3T MRI system. NMR Biomed 2015;28:162–167.
17. Paul J, Divkovic E, Wundrak S, et al. High-resolution respiratory self-gated golden angle cardiac MRI: comparison of self-gating methods in combination with k-t SPARSE SENSE. Magn Reson Med 201;73: 292–298.
18. Motaal AG, Noorman N, De Graaf WL, et al. Functional imaging of murine hearts using accelerated self-gated UTE cine MRI. Int J Cardiovasc Imaging 2015;31:83–94.
19. Hoerr V, Nagelmann N, Nauerth A, Kuhlmann MT, Stypmann J, Faber C. Cardiac-respiratory self-gated cine ultra-short echo time (UTE) cardiovascular magnetic resonance for assessment of functional cardiac parameters at high magnetic fields. J Cardiovasc Magn Reson 2013; 15:59.
20. Trotier AJ, Lefrançois W, Van Renterghem K, Franconi J, Thiaudière E, Miraux S. Positive contrast high-resolution 3D-cine imaging of the cardiovascular system in small animals using a UTE sequence and iron nanoparticles at 4.7, 7 and 9.4 T. J Cardiovasc Magn Reson 2015;17: 53.
21. Sørensen TS, Beerbaum P, Körperich H, Pedersen EM. Three-dimensional, isotropic MRI: a unified approach to quantification and visualization in congenital heart disease. Int J Cardiovasc Imaging 2005;21: 283–292.
22. Riemer F, Solanky BS, Stehning C, Clemence M, Wheeler-Kingshott CA, Golay X. Sodium ((23)Na) ultra-short echo time imaging in the human brain using a 3D-Cones trajectory. MAGMA 2014;27:35–46.
23. Glover GH, Pauly JM, Bradshaw KM. Boron-11 imaging with a three-dimensional reconstruction method. J Magn Reson Imaging 1992;2: 47–52.
24. Irarrazabal P, Nishimura DG. Fast three dimensional magnetic resonance imaging. Magn Reson Med 1995;33:656–662.
25. Boada FE, Gillen JS, Shen GX, Chang SY, Thulborn KR. Fast three dimensional sodium imaging. Magn Reson Med 1997;37:706–715.
26. Gurney PT, Hargreaves BA, Nishimura DG. Design and analysis of a practical 3D cones trajectory. Magn Reson Med 2006;55:575–582.

27. Addy NO, Ingle RR, Wu HH, Hu BS, Nishimura DG. High-resolution variable-density 3D cones coronary MRA. Magn Reson Med 2015;74: 614–621.

28. Kadbi M, Negahdar M, Cha JW, et al. 4D UTE flow: a phase-contrast MRI technique for assessment and visualization of stenotic flows. Magn Reson Med 2015;73:939–950.

29. Winkelmann S, Schaeffter T, Koehler T, Eggers H, Doessel O. An optimal radial profile order based on the golden ratio for time-resolved MRI. IEEE Trans Med Imaging 2007;26:68–76.

30. Beatty PJ, Nishimura DG, Pauly JM. Rapid gridding reconstruction with a minimal oversampling ratio. IEEE Trans Med Imaging 2005;24: 799–808.

31. Kellman P, McVeigh ER. Image reconstruction in SNR units: a general method for SNR measurement. Magn Reson Med 2005;54:1439–1447.

32. Fries P, Massmann A, Seidel R, et al. Comparison of retrospectively self-gated and prospectively triggered FLASH sequences for cine imaging of the aorta in mice at 9.4 Tesla. Invest Radiol 2012;47:259–266.

33. Buonincontri G, Methner C, Krieg T, Carpenter TA, Sawiak SJ. Functional assessment of the mouse heart by MRI with a 1-min acquisition. NMR Biomed 2014;27:733–737.

34. Coppo S, Piccini D, Bonanno G, et al. Free-running 4D whole-heart self-navigated golden angle MRI: initial results. Magn Reson Med 2015;74:1306–1316.

35. Pang J, Bhat H, Sharif B, et al. Whole-heart coronary MRA with 100% respiratory gating efficiency: self-navigated three-dimensional retrospective image-based motion correction (TRIM). Magn Reson Med 2014;71:67–74.

36. Bucholz E, Ghaghada K, Qi Y, Mukundan S, Johnson GA. Four-dimensional MR microscopy of the mouse heart using radial acquisition and liposomal gadolinium contrast agent. Magn Reson Med 2008;60:111–118.

37. Bucholz E, Ghaghada K, Qi Y, Mukundan S, Rockman HA, Johnson GA. Cardiovascular phenotyping of the mouse heart using a 4D radial acquisition and liposomal Gd-DTPA-BMA. Magn Reson Med 2010;63: 979–987.

38. Gharagouzloo CA, McMahon PN, Sridhar S. Quantitative contrast-enhanced MRI with superparamagnetic nanoparticles using ultrashort time-to-echo pulse sequences. Magn Reson Med 2015;74:431–441.

39. Wundrak S, Paul J, Ulrici J, Hell E, Rasche V. A small surrogate for the golden angle in time-resolved radial MRI based on generalized Fibonacci sequences. IEEE Trans Med Imaging 2015;34:1262–1269.

40. Edelman RR, Giri S, Murphy IG, Flanagan O, Speier P, Koktzoglou I. Ungated radial quiescent-inflow single-shot (UnQISS) magnetic resonance angiography using optimized azimuthal equidistant projections. Magn Reson Med 2014;72:1522–1529.

41. Chandarana H, Feng L, Ream J, et al. Respiratory motion-resolved compressed sensing reconstruction of free-breathing radial acquisition for dynamic liver magnetic resonance imaging. Invest Radiol 2015;50: 749–756.

42. Piêdzia W, Jasiñski K, Kalita K, Tomanek B, Wêglarz WP. White and gray matter contrast enhancement in MR images of the mouse brain in vivo using IR UTE with a cryo-coil at 9.4 T. J Neurosci Methods 2014;232:30–35.